Tubulin- and ROS-dependent antiproliferative mechanism of a potent analogue of noscapine, N-propargyl noscapine

Nayana Nambiar, Praveen Kumar Reddy Nagireddy, Ravikumar Pedapati, Srinivas Kantevari, Manu Lopus

PII: S0024-3205(20)30990-5

DOI: https://doi.org/10.1016/j.lfs.2020.118238

Reference: LFS 118238

To appear in: *Life Sciences*

Received date: 1 April 2020

Revised date: 27 July 2020

Accepted date: 5 August 2020

Please cite this article as: N. Nambiar, P.K.R. Nagireddy, R. Pedapati, et al., Tubulin- and ROS-dependent antiproliferative mechanism of a potent analogue of noscapine, N-propargyl noscapine, *Life Sciences* (2020), https://doi.org/10.1016/j.lfs.2020.118238

Tubulin- and ROS-dependent antiproliferative mechanism of a potent analogue of noscapine, N-propargyl noscapine

Nayana Nambiar[1∞], Praveen Kumar Reddy Nagireddy[2∞], Ravikumar Pedapati[2∞], Srinivas Kantevari[2*], and Manu Lopus[1]*

[1]School of Biological Sciences, UM-DAE Centre for Excellence in Basic Sciences, University of Mumbai, Kalina, Mumbai-400098, India

[2]Fluoro & Agrochemicals Division (Organic Chemistry Division-II), CSIR- Indian Institute of Chemical Technology, Hyderabad-500007, Telangana, India

[∞]These authors contributed equally to the work

***Corresponding authors:** School of Biological Sciences, UM-DAE Centre for Excellence in Basic Sciences, University of Mumbai, Kalina, Mumbai-400098, India Email: manu.lopus@cbs.ac.in; Fluoro & Agrochemicals Division (Organic Chemistry Division-II), CSIR-Indian Institute of Chemical Technology, Hyderabad, Telangana-500007, India. Email: ksrinivas@iict.re.sin

Tubulin- and ROS-dependent antiproliferative mechanism of a potent analogue of noscapine, N-propargyl noscapine

ABSTRACT

Aim

To rationally-design, synthesize, characterize, biologically evaluate, and to elucidate the anticancer mechanism of action of a novel analogue of noscapine, N-propargyl noscapine (NPN), as a potential drug candidate against triple-negative breast cancer (TNBC).

Materials and Methods

After the synthesis and IR, ^{1}H, ^{13}C NMR and mass spectral characterization of NPN, its antiproliferative efficacy was investigated against cells of breast cancer (MCF-7 and MDA-MB-231), lung cancer (HOP-62 and A-549), and of a non-cancerous epithelial line (VERO), using the Sulforhodamine B assay. Cell cycle progression was analysed using flow cytometry. The drug-tubulin interactions were studied using tryptophan-quenching assay, ANS-binding assay, and colchicine-binding assay. Immunofluorescence was used to examine the effect of NPN on cellular microtubules. Levels of reactive oxygen species (ROS), loss of mitochondrial membrane potential (MMP), and cell death were studied using staining the cells with DCFDA, Rhodamine 123, and acridine orange/ethidium bromide, respectively.

Key Findings

NPN strongly inhibited the viability (IC_{50}, 1.35 ± 0.2 μM) and clonogenicity (IC_{50}, 0.56 ± 0.06 μM) of the TNBC cell line, MDA-MB-231, with robust G_2/M arrest. NPN showed very little toxicity to the non-cancerous cell line, VERO. In vitro, the drug bound to tubulin and disrupted the latter's structural integrity and promoted colchicine binding to tubulin. NPN triggered an unusual form of microtubule disruption in cells, repressed recovery of cold-depolymerized cellular microtubules and suppressed their dynamicity. These effects on microtubules were facilitated by elevated levels of ROS and loss of MMP.

Significance

NPN can be explored further as a chemotherapeutic agent against TNBC.

1. Introduction

Ever since the discovery of the antitumor potential of noscapine – a benzylisoquinoline alkaloid that belongs to phthalideisoquinoline structural subgroup – in 1998, a plethora of work has been done to develop noscapine-based anticancer therapeutics. The apparent lack of systemic and tissue toxicity, good oral bioavailability, and improved tumor targeting made noscapine and many of its analogs potential therapeutics. Noscapine, for example, has favorable pharmacokinetics (clearance within ~10 h) [1-3] and it lacks toxicity to bone marrow, spleen, kidney, heart, liver, or small intestine [2,3]. These features have prompted preclinical evaluations of noscapine in mouse models of human cancer [3,4] with encouraging results. Although the alkaloid is a constituent isolated from the opium poppy, it is non-narcotic [5] and non-habit forming [5]. Noscapine targets tubulin, the heterodimeric, guanine nucleotide-binding protein that forms the dynamic cytoskeletal filament called microtubules [6]. Among its numerous functions in cells, orchestration of cell cycle progression makes microtubules a potent target for cancer chemotherapy. Interestingly, unlike the majority of antitubulin agents, noscapine neither alter microtubule polymer mass considerably, nor does it grossly damage cellular microtubules [6]. The drug works, instead, by inducing minor alterations on the assembly dynamics of microtubule [7]. However, despite its desirable features, noscapine has never been progressed to cancer clinical trials due to its lack of sufficient toxicity against cancer cells. For example, its IC_{50} against MDA-MB-231 cells is 36 μM [8].

Over the past two decades, several researchers have been focusing on the development of potent noscapine analogues with improved toxicity for cancer chemotherapy. To this end, using structure-activity relationship studies, multiple 'generations' of noscapinoids have been generated with improved cytotoxicity (Fig. 1). Whereas the first-generation analogs have chemical alterations in isoquinoline and benzofuranone ring systems (diversity point B) of the parent compound [9,10], the second generation has had alterations at the diversity point C of the benzofuranone ring system [11]. Isoquinoline ring system at diversity point D was modified to generate the third generation noscapinoids by functionalization of 'N' [12].

Pharmaceuticals having ethyne functionality have gained importance as potent anticancer agents [13]. Drugs, such as Erlotinib(I), Icotinib(II) and 5-Ethynyl-2'-deoxycarbocyclic uridine (III) with ethyne group (Fig. 2), are in commercial use for treating cancer patients. However, the safety profile of these drugs has still been under investigation [14,15]. The N-

propargyl drugs, such as selegiline and parglyline (Fig. 2), were also under investigation against many diseases [16]. In continuation of efforts [17,18] to develop new congeners of α-noscapine for improving the anticancer activity, inclusion of propargyl group on N segment in noscapine core has been explored [19].

In this work, we examined a novel analogue of noscapine rationally-designed noscapinoid, NPN, for its anticancer potential against cell lines representing breast and lung cancers. After a multistep chemical synthesis and an extensive, NMR- and mass spectrometry-assisted structural elucidation of the compound, we employed a combination of cellular-level analyses, biophysical techniques, and in situ imaging to elucidate the anti-proliferative efficacy and mechanism of action of NPN.

2. Materials and Methods

2.1. Materials

Dulbecco's modified Eagle's medium (DMEM), fetal bovine serum (FBS), penicillin and streptomycin, ribonuclease A (RNase A), bovine serum albumin (BSA), trichloroacetic acid (TCA), and horse serum were purchased from HiMedia (Mumbai, India). Rosewell Park Memorial Institute (RPMI-1640) medium, L-glutamine, sulforhodamine B (SRB), dimethyl sulfoxide (DMSO), 8-anilino-1-naphthalenesulfonic acid (ANS), colchicine, guanosine-5′-triphosphate (GTP), glutamate, piperazine-N, N′-bis (2-ethanesulfonic acid) (Pipes), magnesium sulfate ($MgSO_4$), ethylene glycol tetra acetic acid (EGTA), 2′,7′-dichlorofluorescin diacetate (DCFDA), rhodamine 123, propidium iodide, nocodazole, formaldehyde, Taxol, and ethidium bromide were procured from Sigma (St. Louis, MO). Tris buffer, crystal violet and acridine orange from Sisco Research Laboratories Pvt. Ltd. (SRL, Bangalore, India). Prolong Gold antifade reagent and Bradford reagent were obtained from Thermo Scientific, USA. All other reagents were also of analytical grade and highest purity.

2.2. Chemistry

All the reactions were monitored by TLC using precoated silica plates and visualization under UV light. Air-sensitive reagents were transferred by syringe or double-ended needle. Evaporation of solvents was performed at reduced pressure by using heidolph rotary evaporator. ^{1}H and ^{13}C NMR spectra of samples in $CDCl_3$ were recorded on AVANCE-300MHz, 400 MHz, 500 MHz spectrometer (Avance, San Antonio, TX). Chemical shift reported were relative to an internal standard TMS (δ=0.0). Spin multiplicities are described

as s (singlet), brs (broad singlet), d (doublet), t (triplet), q (quartet), or m (multiplet). Coupling constants are reported in hertz (Hz). Mass spectra were recorded in ESI conditions at 70 eV on an Agilent LC-MSD spectrometer (Agilent technologies, Santa Clara, CA). All high-resolution spectra were recorded on QSTAR XL hybrid MS/MS system (Applied Bio systems/ MDS sciex, Foster City, CA), equipped with an ESI source (IICT, Hyderabad). Column chromatography was performed on silica gel (60-120 mesh) supplied by Acme Chemical Co., India. TLC was performed on Merck 60 F-254 silica gel plates. Commercially-available anhydrous solvents dichloromethane, methanol, acetone and ethylacetate were used as such without further purification. Natural α-noscapine was purchased from Sigma.

(*S*)-6,7-dimethoxy-3-((*R*)-4-methoxy-5,6,7,8tetrahydro[1,3]dioxolo[4,5-g]isoquinolin-5yl) isobenzofuran-1(3*H*)-one (4)

Natural α-noscapine 1 (1.0 g, 2.42 mmol) in dichloromethane (10 mL) was added to *m*-CPBA (0.83 g, 4.84 mmol) portion-wise at 0 °C. The reaction mixture was kept for 1h at 25 °C, diluted with dichloromethane (15 mL), and 1M aqueous solution of $NaHSO_3$ (10 mL) was used for the quenching of excess peroxide. The organic layer was separated subsequently, dried with anhydrous Na_2SO_4, and concentrated. The crude residue thus obtained was dissolved in methanol (15 mL), acidified to pH 1.0 using 2N HCl, stirred for 5 min, and filtered. The filtrate was concentrated under reduced pressure, re-dissolved in dichloromethane (15 mL), dried with anhydrous Na_2SO_4, filtered, and concentrated. The pale yellow solid α-noscapine N-oxide.HCl salt thus obtained was dissolved in methanol (20 mL), and $FeSO_4.7H_2O$ (1.34 g, 4.84 mmol) was added into this solution. After stirring the mixture at 25 ºC for 12 h, it was concentrated, and treated with 25% aqueous ammonia to elevate the pH to 10, extracted with dichloromethane (3 x 10 mL), dried with anhydrous Na_2SO_4, and evaporated under reduced pressure. The crude residue, when purified by triethyl amine-treated silica gel column chromatography, and eluted with 4:6 ethyl acetate: hexane, gave (*S*)-6,7-dimethoxy-3-((*R*)-4-methoxy-5,6,7,8 tetrahydro[1,3]dioxolo [4,5-g]isoquinolin-5yl) iso benzofuran-1(3*H*)-one (compound 4; 0.46 g, 48%) as white solid; mp: 171-173 °C; ^{1}HNMR (300 MHz, $CDCl_3$): δ 6.94 (d, *J*= 8.30 Hz, 1H), 6.33 (s, 1H), 5.99-5.89 (m, 4H), 4.85 (d, *J*= 4.53 Hz, 1H), 4.09 (s, 3H), 4.07 (s, 3H), 3.85 (s, 3H), 2.69-2.58 (m, 1H), 2.54-2.42 (m, 1H), 2.36-2.23 (m, 1H), 2.22-2.09 (m, 1H); ^{13}CNMR (75 MHz, $CDCl_3$): δ 168.5, 152.1, 148.3, 147.8, 141.0, 140.4, 134.1, 131.9, 119.6, 118.3, 117.5, 116.9, 103.1, 100.7, 20.6, 62.2, 59.4, 56.6,

52.7, 39.5, 29.7; IR (KBr): 3360, 2942, 1759, 1624, 1501, 1280, 1119, 1074, 1042, 1023, 932, 796, 679 cm^{-1}; MS (ESI): m/z 400 $[M+H]^+$; HRMS (ESI) Calcd for $C_{21}H_{22}NO_7$ $[M+H]^+$: 400.1396, found: 400.1401.

(*S*)-6,7-dimethoxy-3-((*R*)-4-methoxy-6-(prop-2-yn-1-yl)-5,6,7,8-tetrahydro-[1,3]dioxolo[4,5 g]isoquinolin-5-yl)isobenzofuran-1(3*H*)-one (5)

To the solution of compound **4** (0.40 g, 1 mmol) in acetone (10 mL) potassium carbonate (0.41 g, 3.0 mmol), potassium iodide (0.33 g, 2.0 mmol) and propargyl bromide (0.30 mL, 2.0 mmol) were added and stirred at 25 °C for 1 h. After completion of the reaction (as monitored by TLC), the mixture was filtered through celite. After a vacuum-evaporation of the filtrate, the residue was mixed with water (5 mL) and extracted with dichloromethane (2 x 10 mL), combined organic layers were washed with brine, dried over anhydrous Na_2SO_4, and concentrated. The crude extract thus obtained was chromatographed over triethyl amine-treated silica gel column eluting with hexane / ethyl acetate (70:30) to provide compound **5** (0.28 g, 65%) as white solid, mp: 142-144 °C; ^{1}H NMR (500 MHz, $CDCl_3$): δ 6.94 (d, *J* = 8.24 Hz, 1H), 6.31 (s, 1H), 5.98-5.92 (m, 3H), 5.55 (d, *J* = 3.96 Hz, 1H), 4.82 (d, *J* = 3.96 Hz, 1H), 4.08 (s, 3H), 4.07 (s, 3H), 3.93-3.87 (m, 4H), 3.45 (dd, *J* = 1.98, 17.34 Hz, 1H), 2.76-2.67 (m, 1H), 2.62-2.54 (m, 1H), 2.62-2.54 (m, 1H), 2.37-2.28 (m, 1H), 2.11 (t, *J* = 2.13 Hz, 1H), 1.87-1.77 (m, 1H); ^{13}C NMR (125 MHz, $CDCl_3$): δ 167.8, 152.0, 148.3, 147.3, 140.2, 140.1, 134.2, 132.3, 120.1, 117.9, 117.6, 117.1, 102.2, 100.7, 81.9, 80.0, 72.2, 62.0, 59.4, 57.0, 56.5, 47.4, 46.6, 28.9; IR (KBr): 3287, 2928, 2696, 1757, 1626, 1501, 1443, 1430, 1277, 1129, 1033, 1003, 653 cm^{-1}; MS (ESI) *m/z* 438 $[M+H]^+$: HRMS (ESI) Calcd for $C_{24}H_{23}NO_7$ $[M+H]^+$: 438.1547, found: 438.1591.

2.3. Biology

2.3.1. Cell culture

MDA-MB-231 cells were cultured and maintained in DMEM supplemented with 10% (v/v) heat-inactivated fetal bovine serum and penicillin (100U/mL)/streptomycin (0.1mg/mL) solution at 37°C, 5% CO_2, in a Forma Stericycle Incubator (Thermo Fisher, Waltham, MA). MCF-7 (invasive breast ductal carcinoma), HOP-62 (lung adenocarcinoma), A-549 (alveolar basal epithelial cell carcinoma), and VERO (African green monkey kidney epithelial cells) cells were cultured in RPMI 1640 medium (Sigma, St. Louis, MO) containing 10% fetal bovine serum (FBS) and 2 mM L-glutamine.

2.3.2. Cell viability and clonogenicity assays

Effect of NPN on the viability of the cells was studied using a sulforhodamine B (SRB). Briefly, the cells were seeded at a density of 5000 cells/well in poly-L-lysine coated 96-well plates and allowed to attach overnight. Next day, the medium was replaced with fresh medium containing different concentrations of NPN (0–5 µM), and the cells were grown for 72 h. After the incubation, the cells were fixed with 10% TCA for 1 h at 4°C. Subsequently, the wells rinsed with water, air dried, and stained with 0.4% SRB in 1% acetic acid for 1 h. The unbound dye was washed off using 1% acetic acid, and the plates were air dried. The protein-bound SRB was dissolved in 10 mM Tris buffer, and the cell viability was determined by measuring the absorbance at 564 nm using a Tecan Infinite® M200 PRO plate reader (Tecan, Switzerland). The experiment was performed in triplicate and repeated twice. To determine the effect of NPN on each cell in the population for its ability to make colonies, a colony-formation assay was performed. The cells (MDA-MB-231) were seeded in a 6-well cell culture plate at the density of 1000 cells/well, and allowed to attach overnight. Next day, they were treated with NPN (0 µM–1 µM) or nocodazole (1 µM) for 24 h. After the specified time, the medium removed, fresh medium added and the cells were allowed to grow for 8–10 days. The colonies thus formed were fixed with 3.7% formaldehyde and stained with crystal violet, and were imaged and enumerated using ImageJ software (NIH, Bethesda, MD), as described [20]. The experiment was repeated at least twice.

2.3.3. Flow Cytometry

The flow cytometry evaluation of the cell cycle progression was performed as described previously [21], with some modifications. In brief, MDA-MB-231 cells (1 x 10^6 cells/mL) were seeded and allowed to grow in 100-mm tissue culture dishes for 24 h. Next day, the cells were incubated in the presence or absence of NPN (2 µM and 5 µM) or nocodazole (1 µM) for 48 h. At the end of the treatment, the floating and adherent cells were collected, washed with PBS, and fixed with chilled ethanol (70%) by overnight incubation at -20 ºC. After the fixation, the cells washed with PBS and re-suspended in 0.5 mL PBS and treated with RNase A (100 µg/mL) for 30 min at 37˚C and stained with propidium iodide (50 µg/mL). The DNA content was analyzed using BD FACS Aria (BD Bioscience, San Jose, CA) flow cytometer, supported by FACS DIVA software.

2.3.4. Tryptophan-quenching Assay

Tubulin was purified from goat brain by cycles of GTP- and temperature-dependent polymerization and depolymerization cycles, as described [22]. The microtubule-associated protein-free tubulin (MAP-free tubulin) thus purified (2 μM) was incubated with NPN (0–100 μM) or noscapine (50 μM) for 45 min at 35 ˚C in PEM buffer (50 mM Pipes, 1 mM EGTA, 3 mM $MgSO_4$, pH 6.8). The samples were excited at 295 nm, and the emission readings were taken (310–400 nm) in a FlouroMax® 4 spectrofluorometer (Horiba Scientific, Edison, NJ), aided by FluorEssence 3.5 software. The experiment was repeated twice.

2.3.5. ANS-binding assay

Tubulin (2 μM) was incubated first with different concentrations of NPN (0–100 μM) or noscapine (50 μM) for 30 min at 35 °C, and then with 5[illegible] μM freshly-prepared ANS (20 min, 25 ˚C). The fluorescence spectra were recorded from 400 nm to 550 nm after exciting the samples at 380 nm. The assay was repeated twice.

2.3.6. Colchicine-binding assay

Tubulin (3 μM) was incubated with different concentrations of NPN (0–100 μM) or noscapine (50 μM) in PEM buffer at 35˚C for 30 min. After the incubation, colchicine (10 μM) was added to the samples to be incubated further for 1h. After the incubation, the samples were excited at 360 nm, and the emission spectra were recorded 390–550nm. The assay was repeated twice.

2.3.7. Polymer mass assay

Tubulin (12 μM) was assembled on ice in a solution consisting of microtubule assembly buffer (PEM 50, 1 mM GTP, and 1 M glutamate, pH 6.8) in the presence or absence of NPN (0–100μM), noscapine (50 μM) or colchicine (25 μM). The samples were then transferred to 37°C in a temperature- controlled, water-circulating bath and allowed to polymerize for 45 min. After the specified incubation point, the samples were centrifuged in a Beckman Coulter Avanti J26S x P centrifuge (Beckman Coulter, Brea, CA; 28000×g) and the pellet was collected after aspirating off the supernatant. The pelleted protein was incubated with an amount of water equalling to the aspirated off supernatant overnight on ice. The concentration of the protein in each sample was measured by the method of Bradford, using bovine serum albumin as the standard [23].

2.3.8. Visualization of cellular microtubules, their acetylation, and the recovery of microtubule network after cold-induced depolymerization

For immunofluorescence studies, MDA-MB-231 cells were seeded on poly-L-lysine-coated coverslips at a density of 7.5×10^4 cells/well and cultured in the absence or presence of different concentrations of NPN (0–3 µM) for 48 h. The cells were then fixed in 3.7% formaldehyde at 25 ºC for 20 min, washed twice with 1×PBS, and permeabilized with chilled methanol (-20 °C) for 10 min. Non-specific binding sites were blocked by incubating the cells with 5% horse serum in 1× PBS for 1 h at 25 °C. Then, the cells were first incubated with mouse monoclonal anti-α-tubulin antibodies (Sigma; 1:300 dilution) for 1 h at 25 °C, and then with Alexa-568-labeled goat anti-mouse IgG (Molecular Probes; Eugene, CO; 1: 1000 dilution) for 1 h at 25 °C. For examining the effect of NPN on microtubule reassembly after their complete depolymerization, the cells (7.5× 10^5 cells/mL) were grown on the coverslips in a 12-well plate for 24 h without the drug. To depolymerize the microtubules, the plate was incubated on ice for 1 h. After the cold treatment, the media was removed and replaced with fresh, warm, complete media, without or with NPN (2 µM or 3 µM). The cells were then transferred to 37˚C and incubated for 30 min. After the incubation, the cells were stained with anti-tubulin antibodies and the secondary, anti-mouse IgGs, as mentioned earlier. For the visualization of acetylated tubulin, the cells that were grown, treated, fixed, and permeablized as mentioned above were stained with acetyl-α-tubulin (Lys40) antibodies (1:800, Cell Signalling Technology, MA; overnight incubation, 4°C) and FITC-conjugated donkey anti-rabbit antibodies (1:200; Santa Cruz Biotechnology, TX, 2 h; 25°C). The imaging was done using a Nikon Eclipse 90i microscope (Nikon, Tokyo, Japan) equipped with NIS-Elements BR 3.2 software.

2.3.9. Detection of reactive oxygen species and mitochondrial membrane potential

Intracellular ROS production in the presence and absence of NPN was examined using the fluorescence probe, 2',7'-dichlorodihydrofluorescein diacetate (DCFDA) which fluoresces green when oxidized to 2 ,7 -dichlorofluorescein (DCF), as described previously [24]. In brief, 5×10^4 cells were grown on poly-L-lysine-coated coverslip with or without NPN (2 µM or 3µM) for 24 h. After exposure to the drug, the cells were incubated with DCFDA (50 µM) for 30 min at 37°C. The cells were then washed with PBS, and observed under a Nikon Eclipse 90i fluorescence microscope (Nikon, Tokyo, Japan). The increased level of fluorescence intensity is indicative of the increased ROS generation. H_2O_2 (400 µM) was

used as the positive control. The experiment was repeated once. The effect of the drug on mitochondrial membrane integrity was examined by observing the changes in the fluorescence intensity of rhodamine 123, a cationic fluorescent dye that labels respiring mitochondria. Briefly, 5×10^4 cells/mL were seeded on poly-L-lysine-coated coverslips with or without NPN (2 µM or 3µM) for 24 h. The cells were then incubated with rhodamine 123 (10 µg/mL) for 30 min at 37°C. Subsequently, the cells were washed with PBS, and observed under the Nikon TS-100 microscope. The fluorescence intensity of the cells was quantified using Image J [25].

2.3.10. Detection of cell death

The ability of the drug to induce cell death was examined as follows. The cells, seeded at a density of 5×10^4 cells/mL and treated the next day with or without NPN (2 µM and 3 µM) or nocodazole (1 µM) for 48 h were dual stained with 10 µg/mL of acridine orange and 10 µg/ml of ethidium bromide. The cells were then washed with PBS to remove the excess stain and viewed under the Nikon TS-100 fluorescence microscope. About 200 cells were examined, and the percentage of cells depicting the morphological changes enumerated. The treated cells were quantified according to the following descriptions: (1) Normal nuclei (bright-green chromatin, organised structure), (2) early phase of death (bright-green chromatin, condensed or fragmented), (C) late stage of death (bright orange chromatin, highly condensed or fragmented) and (D) dead/necrotic (deep red cells).

2.3.11. Statistical analysis

All measurements were made in triplicates and the values plotted as mean ± standard deviation. Students' t-test was used to analyse the data. The data were considered statistically significant at 0.05 level of confidence.

3. Results

3.1. Chemistry

α-Noscapine **1** structurally consists of two major constituents, isoquinoline and pthalide ring systems, connected with a sensitive C-C bond, which is labile to strong acids and bases. Therefore, the synthesis of noscapine analogues is challenging. In the present work, we have optimized the reaction conditions for the synthesis of noscapinoids without affecting the sensitive C-C bond. The design and synthetic approach for the preparation of N-propargyl noscapine (**5)** is depicted in Fig. 3. Commercial noscapine (**1**) was treated with *meta*-

chloroperbenzoic acid (*m*-CPBA) and acidified to yield the respective N-oxide hydrochloride salt. The salt was further reacted using $FeSO_4.7H_2O$ (under modified non-classical Polonovski reaction conditions) to synthesize the penultimate compound (**4**) (nornoscapine) in 48% overall yields [12,26,27]. In the next step, (S)-6,7-dimethoxy-3-((R)-4-methoxy-6-(prop-2-yn-1-yl)-5,6,7,8-tetrahydro-[1,3]dioxolo[4,5-g] isoquinolin-5-yl)isobenzofuran-1(3H)-one (**4**) were obtained by the reaction of propargyl bromide with K_2CO_3 and KI in acetone at RT for 1h. After completion, the contents were partitioned between water and dichloromethane. The organic layer was collected, removed in vacuo, and flash chromatography with hexane/ethyl acetate (70:30) gave good yields (65%) of the desired N-propargyl derivative. The product **5** was fully characterized by IR, ^{1}H & ^{13}C NMR and Mass (ESI and HRMS) spectral data (Supplementary Fig. 1 A-C).

3.2. Biology

3.2.1. NPN is a potent antiproliferative, anti-clonogenic, and cell cycle-arresting noscapinoid

We started the investigations by examining the relative antiproliferative efficacy of NPN on a variety of cancer cell lines including, MDA-MB-231 (triple-negative breast cancer), MCF-7 (invasive breast ductal carcinoma), HOP-62 (lung adenocarcinoma), A-549 (alveolar basal epithelial cell carcinoma), and a non-cancerous cell line, VERO (African green monkey kidney epithelial cells). The noscapinoid preferentially inhibited the proliferation of the cancer cell lines in a concentration-dependent manner (Supplementary Table 1). MDA-MB-231 cells responded most favorably to the drug by reducing their viability with an IC_{50} of 1.35 ± 0.2 µM. MCF-7, HOP-62, and A-549 were less responsive with IC_{50}s, 75 ± 1 µM, 15.6 ± 0.6 µM, and 87 ± 4 µM, respectively. The non-cancerous cell line, VERO, respond poorly to the drug with an IC_{50} above 100 µM. Having identified NPN's preferential inhibition of MDA-MB-231 cells (Fig. 4A), we performed further cell model analyses on this cell line. A colony-formation assay showed strong inhibition of the clonogenic propagation of MDA-MB-231 cells by the drug at nanomolar range. For example, compared with the control, 100 nM, 500 nM, and 1000 nM of NPN decreased the number of colonies by 8%, 45% and 77%, respectively, yielding an IC_{50} of 560 ± 60 nM (Fig. 4 B & C). As revealed by a flow cytometry analysis, NPN arrested MDA-MB-231's cell cycle at the G_2/M phase in a concentration-dependent manner (Fig. 4D). Specifically, compared to the control, 2 µM and 5 µM NPN showed 46% and 56% increase in cells that are at G_2/M phase, respectively, indicating that the antiproliferative mechanism of NPN involves G_2/M arrest. (Fig. 4 D&E).

3.2.2. Direct binding interactions of NPN with purified tubulin and its effect on tubulin assembly

After verifying the potency of NPN on MDA-MB-231 cells, we checked for the potential binding interactions of NPN with tubulin, a prominent target for several breast cancer drugs. Using a tryptophan-quenching assay, it was observed that NPN binds to tubulin in a concentration-dependent manner (Fig. 5A). For example, compared to the control, 25 µM and 100 µM of the drug quenched the intrinsic tryptophan fluorescence by 26% and 59%, respectively. Using an ANS-binding assay, it was found that the drug induces considerable loss of the structural integrity of tubulin (Fig. 5B). For example, 25 µM and 100 µM NPN increased the tubulin-ANS fluorescence by 13% and 28%, respectively, indicating that NPN alters the tertiary conformation of the protein. To gain further understanding of its nature of binding, we performed a colchicine-binding assay. NPN did not inhibit colchicine binding to tubulin but, as Fig. 5C shows, it promoted colchicine-tubulin fluorescence in a concentration-dependent manner. For example, 25 µM and 100 µM of NPN showed 4% and 39% increase in tubulin-colchicine fluorescence. The results suggest a slight alteration of colchicine binding site on tubulin by NPN to promote the binding of colchicine to tubulin. Next, we examined whether these interactions translated into a reduced polymer mass of the assembled tubulin. Interestingly, NPN, even at 100 µM, did not alter the microtubule polymer mass significantly (Fig. 5D).

3.2.3. Effect of NPN on the architecture, reassembly, and dynamicity of cellular microtubules

After examining NPN's interactions with purified tubulin, we tested the impact of these interactions on microtubule in MDA-MB-231 cells. Immunofluorescence imaging of untreated cells showed well-organized microtubule network. NPN, near its IC_{50} for cell viability, rearranged the microtubules in a peculiar fashion. Specifically, keeping some of the microtubules intact, the drug decorated the peripheral regions of the network with clusters of tubulin (Fig. 6A). When the drug concentration was doubled, the damage became more pronounced with an increase in the number of clusters and an apparent reduction in the circumference of the network. The positive control, nocodazole, showed near-complete depolymerization of the microtubules. Investigating further into its microtubule-targeted mechanism in cells, we found that the drug debilitates tubulin's ability to re-establish a structurally-intact network after cold-induced, total disassembly of the microtubules (Fig. 6B). Specifically, compared to the control cells that could reorganize their microtubule

network with a 30-min continuous incubation at 37 ºC after the cold treatment, NPN (2 µM) kept the tubulin depolymerized under identical conditions. Next, we wanted to know whether the drug treatment altered the dynamicity of the microtubules. Acetylation pattern of the microtubules is an indicator of persistent stability of microtubule. The drug-treated microtubules showed considerable tubulin acetylation compared to the control cells (Fig. 6C), indicating that the drug suppressed the dynamicity of the microtubules.

3.2.4. Elevation of ROS and loss of mitochondrial membrane potential, and induction of cell death

We then investigated further into the antiproliferative mechanism of action of NPN by checking the levels of ROS as an elevation of ROS level beyond the physiological range is known to kill the cells. Using a classic DCFDA assay, we detected high levels of ROS in the drug-treated cells, indicating the involvement of ROS in NPN-mediated apoptosis. Specifically, compared to the control cells, cells treated with 2 µM and 3 µM NPN showed 2.5-fold and 3-fold increases in DCF fluorescence intensity (Fig. 7 A & D), indicating the elevated level of ROS in cells. The treated cells also showed an apparent decrease (71% reduction) in rhodamine 123 fluorescence at 2 µM NPN and a 77% decrease at 3 µM of the drug, compared to the control cell (Fig. 7 B & E), suggesting a concentration-dependent loss of mitochondrial membrane potential. NPN treatment promoted cell death in MDA-MB-231 cells. To examine the cell death, we used the classical acridine orange-ethidium bromide staining method. Acridine orange emits is taken up by both viable and non-viable cells, whereas ethidium bromide, is taken up only by the non-viable cells. At 2 µM NPN, 35% cells were found to be undergoing cell death and at 3 µM, 84% of the cells were found to be undergoing death (Fig. 7 C & F).

4. Discussion

The ability of noscapine to preferentially target tumour cells while leaving normal tissues intact makes it a potential anticancer agent [6]. Efforts to improve its cytotoxic efficacy have resulted in the development of multiple generations of noscapinoids with modifications at different locations on the core noscapine architecture (Fig. 1). With insights from the efficacy of ethyne and N-propargyl group-containing molecules (Fig. 2), here, we report a new design strategy that yielded a noscapinoid (NPN; Fig. 3) which is 26-times more efficacious than the parent compound [8] against triple-negative breast cancer cells, and elucidate its tubulin-targeted mechanism of action using biophysical, biochemical, and cellular-level analyses.

4.1. Antiproliferative and anti-clonogenic efficacy of NPN against MDA-MB-231 cells

Among the cancer cell lines (MCF-7, MDA-MB-231, HOP-62, A-549) and the non-cancerous cell line (VERO) tested, NPN showed the highest potency against the viability of MDA-MB-231 cells, indicating its preferential cytotoxicity (Fig. 4A; Supplementary Table 1) against this breast cancer cell line. Further, its apparent lack of considerable toxicity against the non-cancerous cell line VERO (Supplementary Table 1) substantiates the general feature of noscapine-based compounds as preferentially toxic to cancer cells [6]. Compared to the parent compound that inhibits MDA-MB-231 cell proliferation with an IC_{50} of ~ 36 μM [8], this rationally designed analogue is ~26-times more potent in its antiproliferative efficacy. In further support of its anticancer efficacy, the compound inhibited clonogenicity of the cells at nanomolar concentrations (Fig. 4B&C). Aggressive cancers, such as the TNBC, propagate and metastasize by making new colonies in the body. NPN, with its strong inhibition of the clonal expansion of the cells, holds therapeutic potential in this regard. We next wanted to pinpoint the phase of the cell cycle at which the noscapinoid exerts its influence. This investigation was particularly important because different noscapine analogues are known to arrest cell cycle at different phases [26-28]. Whereas noscapine arrests cells in G_2/M phase [28], its analogues like VinPhe-Nos induces S-phase arrest [29]. NPN arrested cell cycle at G_2/M phase (Fig. 4 D&E), thus displaying similarity to the parent compound and to the majority of anti-tubulin agents.

Noscapinoids are known for their binding interactions with tubulin. To verify whether the structural alterations with which NPN was created affected its tubulin binding ability, we performed a collection of classic tubulin-binding analyses using purified goat-brain tubulin. Indicating retention of the tubulin-binding ability of noscapine, NPN showed a concentration-dependent quenching of the intrinsic tryptophan fluorescence of tubulin (Fig. 5A). Further, the ANS binding assay showed that the binding is sufficient to perturb the tertiary conformation of the protein (Fig. 5B). ANS is a fluorescent probe whose fluorescence increases with binding to exposed hydrophobic patches on a protein [19]. Thus, the antiproliferative mechanism of this novel analogue involves binding to tubulin and perturbation of the latter's tertiary conformation. To gain further insight into the nature of binding of NPN to tubulin, we performed a colchicine-binding assay in which, after incubating tubulin with NPN, the samples were incubated further with colchicine. Drugs that preferentially bind colchicine site reduce the colchicine binding to tubulin in a concentration-dependent manner as will be indicated by a reduction in tubulin-colchicine fluorescence.

NPN, on the contrary, enhanced the tubulin-colchicine fluorescence (Fig. 5C), indicating that the drug-induced conformational change in the protein promotes colchicine binding to tubulin. Despite its direct binding to tubulin, NPN did not affect the microtubule polymer mass considerably (Fig. 5D), demonstrating that the drug follows the general modality of action of noscapine congeners on microtubule polymer mass [30].

4.2. An unusual manifestation of microtubule perturbation, inhibition of microtubule recovery, and persistent stabilization of the microtubules in cells

After confirming its direct targeting of tubulin and assessing its impact on *in vitro* tubulin assembly, we wanted to know how these binding interactions transform or disrupt cellular microtubules. Using immunofluorescence visualization of the drug-treated microtubules, we observed a strange rearrangement of the microtubule network. Unlike the microtubules of the control cells where the network was well organized with defined peripheries, the drug-treated cells showed a firework-like arrangement–specifically, that of the "aerial-star-shell" type – in which microtubules near the cell's periphery appeared as multiple clusters with apparent perturbation of the network (Fig. 6A). Thus, unlike any of the past analogues of noscapine, NPN brought forth a novel rearrangement of cellular microtubules. In fact, the majority of noscapinoids examined to date showed only slight damage to cellular microtubules [6], making NPS an exceptional novel analogue. NPN's tubulin-targeted action also involved inhibition of reassembly of disassembled microtubules. Specifically, it was found that the drug debilitated the temperature-dependent reassembly capacity of tubulin after cold-induced total disassembly of the cellular microtubule network (Fig. 6B). This observation suggests that the direct binding of NPN to tubulin is able to suppress the assembly competence of the protein. Investigating further into its microtubule-targeted mechanism of action, it was found that the alkaloid enhances the acetylation pattern of microtubules (Fig. 6C). Hyper-acetylated microtubules are a sign of their persistent stability. In other words, acetylated microtubules generally show suppressed dynamicity [31]. Therefore, like the current tubulin-targeted cancer therapeutics in the market [32], NPN is a potent suppressor of microtubule dynamics.

4.3. The relationship between ROS generation and disruption of microtubules

Next, we set out to further elucidate the mechanism behind the drug-induced disruption of microtubule assembly, reassembly, and dynamics. Given that NPN did not inhibit the polymer mass of in vitro tubulin assembly (Fig. 5D), we expected negligible impact of the drug on cellular microtubules. Interestingly, as described above, the drug strongly disrupted

the microtubule network, inhibited its reassembly, and suppressed the dynamicity of the microtubules (Fig. 6). Therefore, there must exist mechanisms that complemented the microtubule-targeted action of NPN. The loss of mitochondrial membrane potential and elevated ROS levels in the-dug treated cells (Fig. 7 A&D and B&E)) suggested the involvement of ROS in complimenting the microtubule-targeted effects of NPN. Oxidative stress can indeed damage cellular microtubules [33]. Moreover, by preventing free tubulin from assembling, ROS could contribute to the inhibition of the reassembly of microtubules [34], as observed (Fig. 6B). ROS is known to interfere with microtubule dynamics as well [35]. Specifically, with its 20 Cys residues, the α-β tubulin heterodimer is susceptible to oxidation by the ROS [36]. Therefore, while normal polymerization of tubulin can be facilitated by physiological levels of ROS, abnormally high level of ROS can interfere with the natural assembly dynamics tubulin through oxidization of its thiol groups [37]. Thus, NPN, in addition to its direct targeting of tubulin and microtubules, suppressed the microtubule dynamicity (Fig. 6C), at least in part, by elevating the ROS level in the cells. So, how tubulin, the target of the drug, could contribute to the generation of ROS? Tubulin regulates mitochondrial membrane potential by interacting with the mitochondrial channels [38]. By targeting tubulin, NPN could deplete the competency of tubulin to effectively guard these channels. The mitochondria, thus made dysfunctional, generate even more ROS [39], and the ROS thus elevated could further deteriorate mitochondrial function [40].

It is worth mentioning that, for the parent compound noscapine that progressed to clinical trials for lymphoma (https://clinicaltrials.gov/ct2/show/NCT00183950), the IC_{50} of the compound against the lymphoma cells line was 10 μM [2]. With approximately 27 times lesser IC_{50} than the parent compound against MDA-MB-231 cells, we believe NPN holds considerable clinical potential to progress to clinical trials – provided it shows efficacy in preclinical animal models studies. Moreover, as we and others had shown earlier [2,41], due to the safe pharmacological profiles of noscapine and its analogues, higher doses might be possible without encountering dose-limiting side effects. Taken together, our findings suggest that NPN is a potent tubulin-targeted anticancer agent that can be investigated for their anticancer efficacy in preclinical models.

5. References

[1] P.K. Naik, M. Lopus, R. Aneja, S.N. Vangapandu, H.C. Joshi, In silico inspired design and synthesis of a novel tubulin-binding anti-cancer drug: Folate conjugated noscapine (Targetin), J. Comput. Aided Mol. Des. 26 (2012) 233–247.

https://doi.org/10.1007/s10822-011-9508-z.

[2] Y. Ke, K. Ye, H.E. Grossniklaus, D.R. Archer, H.C. Joshi, J.A. Kapp, Noscapine inhibits tumor growth with little toxicity to normal tissues or inhibition of immune responses, Cancer Immunol. Immunother. 49 (2000) 217–225. https://doi.org/10.1007/s002620000109.

[3] J.W. Landen, R. Lang, S.J. McMahon, N.M. Rusan, A.M. Yvon, A.W. Adams, M.D. Sorcinelli, R. Campbell, P. Bonaccorsi, J.C. Ansel, D.R. Archer, P. Wadsworth, C.A. Armstrong, H.C. Joshi, Noscapine alters microtubule dynamics in living cells and inhibits the progression of melanoma, Cancer Res. 62 (2002) 4109–4114.

[4] K. Ye, Y. Ke, N. Keshava, J. Shanks, J.A. Kapp, R.R. Tekmal, J. Petros, H.C. Joshi, Opium alkaloid noscapine is an antitumor agent that arrests metaphase and induces apoptosis in dividing cells, Proc. Natl. Acad. Sci. U. S. A. 95 (1998) 1601–1606. https://doi.org/10.1073/pnas.95.4.1601.

[5] A.E. Robinson, Martindale: The Extra Pharmacopoeia 27th Edition*, J. Pharm. Pharmacol. 29 (1977) 647–648. https://doi.org/10.1111/j.2042-7158.1977.tb11428.x.

[6] M. Lopus, P.K. Naik, Taking aim at a dynamic target: Noscapinoids as microtubule-targeted cancer therapeutics, Pharmacol. Reports. 67 (2015) 56–62. https://doi.org/10.1016/j.pharep.2014.09.003.

[7] J. Zhou, D. Panda, J.W. Landen, L. Wilson, H.C. Joshi, Minor alteration of microtubule dynamics causes loss of tension across kinetochore pairs and activates the spindle checkpoint, J. Biol. Chem. 277 (2002) 17200–17208. https://doi.org/10.1074/jbc.M110360200.

[8] M.B. Chougule, A.R. Patel, T. Jackson, M. Singh, Antitumor activity of Noscapine in combination with doxorubicin in triple negative breast cancer, PLoS One. 6 (2011). https://doi.org/10.1371/journal.pone.0017733.

[9] R. Aneja, S.N. Vangapandu, M. Lopus, R. Chandra, D. Panda, H.C. Joshi, Development of a novel nitro-derivative of noscapine for the potential treatment of drug-resistant ovarian cancer and T-cell lymphoma, Mol. Pharmacol. 69 (2006) 1801–1809. https://doi.org/10.1124/mol.105.021899.

[10] R. Aneja, S.N. Vangapandu, M. Lopus, V.G. Viswesarappa, N. Dhiman, A. Verma, R. Chandra, D. Panda, H.C. Joshi, Synthesis of microtubule-interfering halogenated noscapine analogs that perturb mitosis in cancer cells followed by cell death, Biochem. Pharmacol. 72 (2006) 415–426. https://doi.org/10.1016/j.bcp.2006.05.004.

[11] R.C. Mishra, P. Karna, S.R. Gundala, V. Pannu, R.A. Stanton, K.K. Gupta, M.H. Robinson, M. Lopus, L. Wilson, M. Henary, R. Aneja, Second generation benzofuranone ring substituted noscapine analogs: Synthesis and biological evaluation, Biochem. Pharmacol. 82 (2011) 110–121. https://doi.org/10.1016/j.bcp.2011.03.029.

[12] N.K. Manchukonda, P.K. Naik, S. Santoshi, M. Lopus, S. Joseph, B. Sridhar, S. Kantevari, Rational design, synthesis, and biological evaluation of third generation α-noscapine analogues as potent tubulin binding anti-cancer agents, PLoS One. 8 (2013). https://doi.org/10.1371/journal.pone.0077970.

[13] J. Lehmann, M.H. Wright, S.A. Sieber, Making a Long Journey Short: Alkyne Functionalization of Natural Product Scaffolds, Chem. - A Eur. J. 22 (2016) 4666–

4678. https://doi.org/10.1002/chem.201504419.

[14] G.L. Fekete, L. Fekete, Cutaneous leukocytoclastic vasculitis associated with erlotinib treatment: A case report and review of the literature, Exp. Ther. Med. 17 (2019) 1128–1131. https://doi.org/10.3892/etm.2018.6988.

[15] Y. Wang, C. Zhou, G. Schmid Bindert, Erlotinib in the treatment of advanced non-small cell lung cancer: An update for clinicians, Ther. Adv. Med. Oncol. 4 (2012) 19–29. https://doi.org/10.1177/1758834011427927.

[16] N.J. Ives, R.L. Stowe, J. Marro, C. Counsell, A. Macleod, C.E. Clarke, R. Gray, K. Wheatley, Monoamine oxidase type B inhibitors in early Parkinson's disease: Meta-analysis of 17 randomised trials involving 3525 patients, Br. Med. J. 329 (2004) 593–596. https://doi.org/10.1136/bmj.38184.606169.AE.

[17] P.K. Reddy Nagireddy, V.K. Kommalapati, N.K. Manchikonda, B. Sridhar, A.D. Tangutur, S. Kantevari, Synthesis and Antiproliferative Activity of 9-Formyl and 9-Ethynyl Noscapines, ChemistrySelect. 4 (2019) 4092–4096. https://doi.org/10.1002/slct.201900666.

[18] P.K.R. Nagireddy, B. Sridhar, S. Kantevari, Copper-Catalyzed Glaser-Hey-Type Cross Coupling of 9-Ethynyl-α-Noscapine Leading to Unsymmetrical 1,3-Diynyl Noscapinoids, Asian J. Org. Chem. 8 (2019) 1493–1500. https://doi.org/10.1002/ajoc.201900316.

[19] S. Cheriyamundath, T. Mahaddalkar, P.K. Reddy Nagireddy, B. Sridhar, S. Kantevari, M. Lopus, Insights into the structure and tubulin-targeted anticancer potential of N-(3-bromobenzyl) noscapine, Pharmacol. Reports. 71 (2019) 48–53. https://doi.org/10.1016/j.pharep.2018.09.002.

[20] T. Mahaddalkar, S. Mehta, S. Cheriyamundath, H. Muthurajan, M. Lopus, Tryptone-stabilized gold nanoparticles target tubulin and inhibit cell viability by inducing an unusual form of cell cycle arrest, Exp. Cell Res. 360 (2017) 163–170. https://doi.org/10.1016/j.yexcr.2017.09.002.

[21] T. Mahaddalkar, N. Manchukonda, S. Choudhary, S. Cheriyamundath, N. Mohanpuria, S. Kantevari, M. Lopus, Subtle Alterations in Microtubule Assembly Dynamics by Br-TMB-Noscapine Strongly Suppress Triple-Negative Breast Cancer Cell Viability Without Mitotic Arrest, ChemistrySelect. 1 (2016) 4313–4319. https://doi.org/10.1002/slct.201600959.

[22] M. Pradhan, C. Suri, S. Choudhary, P.K. Naik, M. Lopus, Elucidation of the anticancer potential and tubulin isotype-specific interactions of β-sitosterol, J. Biomol. Struct. Dyn. 36 (2018) 195–208. https://doi.org/10.1080/07391102.2016.1271749.

[23] M.M. Bradford, A rapid and sensitive method for the quantitation of microgram quantities of protein utilizing the principle of protein-dye binding, Anal. Biochem. 72 (1976) 248–254. https://doi.org/10.1016/0003-2697(76)90527-3.

[24] A. Aranda, L. Sequedo, L. Tolosa, G. Quintas, E. Burello, J. V. Castell, L. Gombau, Dichloro-dihydro-fluorescein diacetate (DCFH-DA) assay: A quantitative method for oxidative stress assessment of nanoparticle-treated cells, Toxicol. Vitr. 27 (2013) 954–963. https://doi.org/10.1016/j.tiv.2013.01.016.

[25] E.C. Jensen, Quantitative Analysis of Histological Staining and Fluorescence Using

ImageJ, Anat. Rec. 296 (2013) 378–381. https://doi.org/10.1002/ar.22641.

[26] A.J. Debono, S.J. Mistry, J. Xie, D. Muthiah, J. Phillips, S. Ventura, R. Callaghan, C.W. Pouton, B. Capuano, P.J. Scammells, The synthesis and biological evaluation of multifunctionalised derivatives of noscapine as cytotoxic agents, ChemMedChem. 9 (2014) 399–410. https://doi.org/10.1002/cmdc.201300395.

[27] A.J. Debono, J.H. Xie, S. Ventura, C.W. Pouton, B. Capuano, P.J. Scammells, Synthesis and Biological Evaluation of N-Substituted Noscapine Analogues, ChemMedChem. 7 (2012) 2122–2133. https://doi.org/10.1002/cmdc.201200365.

[28] S. Sajadian, M. Vatankhah, M. Majdzadeh, S.M. Kouhsari, M.H. Ghahremani, S.N. Ostad, Cell cycle arrest and apoptogenic properties of opium alkaloids noscapine and papaverine on breast cancer stem cells, Toxicol. Mech. Methods. 25 (2015) 388–395. https://doi.org/10.3109/15376516.2015.1045656.

[29] S. Cheriyamundath, T. Mahaddalkar, S. Kantevari, M. Lopus, Induction of acetylation and bundling of cellular microtubules by 9-(4-vinylphenyl) noscapine elicits S-phase arrest in MDA-MB-231 cells, Biomed. Pharmacother. 85 (2017) 74–80. https://doi.org/10.1016/j.biopha.2016.11.143.

[30] T. Mahaddalkar, P.K. Naik, S. Choudhary, N. Manchukonda, S. Kantevari, M. Lopus, Structural investigations into the binding mode of a novel noscapine analogue, 9-(4-vinylphenyl) noscapine, with tubulin by biochemical analyses and molecular dynamic simulations, J. Biomol. Struct. Dyn. 35 (2017) 2475–2484. https://doi.org/10.1080/07391102.2016.1222969.

[31] M.A. Badding, D.A. Dean, Highly acetylated tubulin permits enhanced interactions with and trafficking of plasmids along microtubules, Gene Ther. 20 (2013) 616–624. https://doi.org/10.1038/gt.2012.77.

[32] T. Mahaddalkar, M. Lopus, From Natural Products to Designer Drugs: Development and Molecular Mechanism of Action of Novel Anti-Microtubule Breast Cancer Therapeutics, Curr. Top. Med. Chem. 17 (2017) 2559 - 2568. https://doi.org/10.2174/1568026617666170104144240.

[33] C.F. Lee, C.Y. Lin, K.H. Hsieh, Y.H. Wei, Oxidative stress-induced depolymerization of microtubules and alteration of mitochondrial mass in human cells, Ann. N. Y. Acad. Sci. 1042 (2005) 246–254. https://doi.org/10.1196/annals.1338.027.

[34] H. Hess, J.L. Ross, Non-equilibrium assembly of microtubules: From molecules to autonomous chemical robots, Chem. Soc. Rev. 46 (2017) 5570–5587. https://doi.org/10.1039/c7cs00030h.

[35] M.S. Islam, A.M.R. Kabir, D. Inoue, K. Sada, A. Kakugo, Enhanced dynamic instability of microtubules in a ROS free inert environment, Biophys. Chem. 211 (2016) 1–8. https://doi.org/10.1016/j.bpc.2015.11.003.

[36] L.M. Landino, R. Hasan, A. McGaw, S. Cooley, A.W. Smith, K. Masselam, G. Kim, Peroxynitrite oxidation of tubulin sulfhydryls inhibits microtubule polymerization, Arch. Biochem. Biophys. 398 (2002) 213–220. https://doi.org/10.1006/abbi.2001.2729.

[37] L.M. Landino, M.T. Koumas, C.E. Mason, J.A. Alston, Modification of tubulin cysteines by nitric oxide and nitroxyl donors alters tubulin polymerization activity,

Chem. Res. Toxicol. 20 (2007) 1693–1700. https://doi.org/10.1021/tx7001492.

[38] E.N. Maldonado, J. Patnaik, M.R. Mullins, J.J. Lemasters, Free tubulin modulates mitochondrial membrane potential in cancer cells, Cancer Res. 20 (2010) 10192–10201. https://doi.org/10.1158/0008-5472.CAN-10-2429.

[39] J. Ježek, K.F. Cooper, R. Strich, Reactive oxygen species and mitochondrial dynamics: The yin and yang of mitochondrial dysfunction and cancer progression, Antioxidants. 7 (2018). https://doi.org/10.3390/antiox7010013.

[40] Z. Li, S. Chen, K. Ma, X. Lv, H. Lin, B. Hu, R. He, Z. Shao, CsA attenuates compression-induced nucleus pulposus mesenchymal stem cells apoptosis via alleviating mitochondrial dysfunction and oxidative stress, Life Sci. 205 (2018) 26–37. https://doi.org/10.1016/j.lfs.2018.05.014.

[41] R. Aneja, M. Lopus, J. Zhou, S.N. Vangapandu, A. Ghaleb, J. Yao, J.H. Nettles, B. Zhou, M. Gupta, D. Panda, R. Chandra, H.C. Joshi. Rational design of the microtubule-targeting anti-breast cancer drug EM015. Cancer Res. 66 (2006) 3782–3791. doi: 10.1158/0008-5472.CAN-05-2962

Figure Legends

Figure 1. Natural α-noscapine and its congeners

Figure 2. Ethyne and N-propargyl group-containing bioactive molecules

Figure 3 A**.** Design strategy of NPN. B. Synthesis of N-propargyl noscapine: Reaction Conditions. (i) a: mCPBA, DCM; b: 2N HCl; c: $FeSO_4.7H_2O$; (ii) Propargyl bromide, K_2CO_3, KI, acetone, 25 º, 1h, 65%

Figure 4. Effects of NPN on cell viability, clonogenicity, and cell cycle progression A. Inhibition of MDA-MB-231 cell viability by NPN as determined using SRB assay. B&C. Inhibition of colony formation of MDA-MB-231 cells by NPN. The graph is presented as mean ± SD, n=3, and considered significant if *p< 0.05, **p< 0.01, ***p < 0.001 compared to the control. D&E. Inhibition of cell cycle progression at the G_2/M phase. *Noco*-nocodazole, *C*, control

Figure 5. Interactions of NPN with pure Tubulin. A. NPN decreased the intrinsic tryptophan fluorescence of tubulin in a concentration-dependent manner. B. Perturbation of the tertiary structure of tubulin by NPN as evidenced by the concentration-dependent increase in tubulin-ANS fluorescence. C. Potential stabilization of colchicine binding to tubulin by NPN as indicated by the concentration-dependent increase in tubulin-colchicine fluorescence. D.

Lack of inhibition of in vitro polymer mass of microtubules by NPN. A-C, the graph is a representative of two independent experiments. D, the graph represents mean ± SD, n=3; the data are considered significant at *p< 0.05, compared to the control. *Nos*, noscapine; *Noco*, nocodazole; *Col*, colchicine.

Figure 6. Effects of NPN on cellular microtubules. A. Microtubules of MDA-MB-231 cells treated with NPN displaying disruption of the normal arrangement of microtubules. B. NPN inhibited the recovery of cold-induced depolymerized microtubules. C. Extensive acetylation of cellular microtubules induced by NPN, indicating the loss of the dynamicity.

Figure 7. Concentration-dependent effect of NPN on ROS, MMP and induction of cell death. A &D. Representative images and bar graphs representing the pixel intensity of DCF fluorescence, indicating elevated levels of ROS in the drug-treated cells. B & E. Loss of mitochondrial membrane potential in NPN-treated MDA-MB-231 cells as indicated by the rhodamine 123 fluorescence. C & F. Visualization of apoptotic cells in MDA-MB-231 showing an increase in the percentage of dead cells with increasing drug concentration. Data are obtained from three independent experiments. Two hundred cells were analysed for each condition. The bar graphs represents the mean ± SD (n = 2), and considered significant at the observed values (**p< 0.01, ***p < 0.001), compared to the control. *Noco*- nocodazole, H_2O_2, Hydrogen peroxide.

Figures

Figure 1

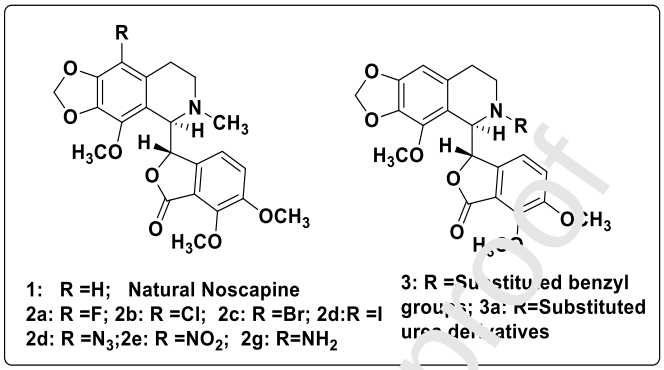

Figure 2

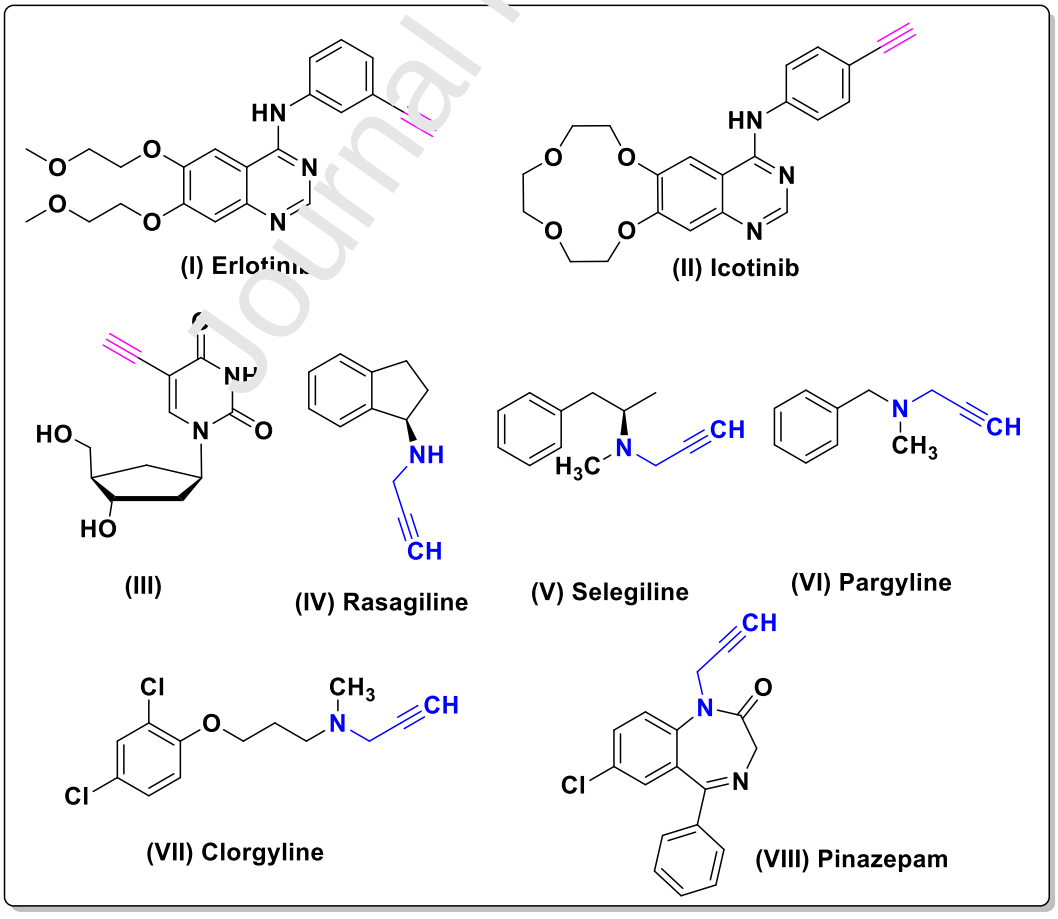

Figure 3A

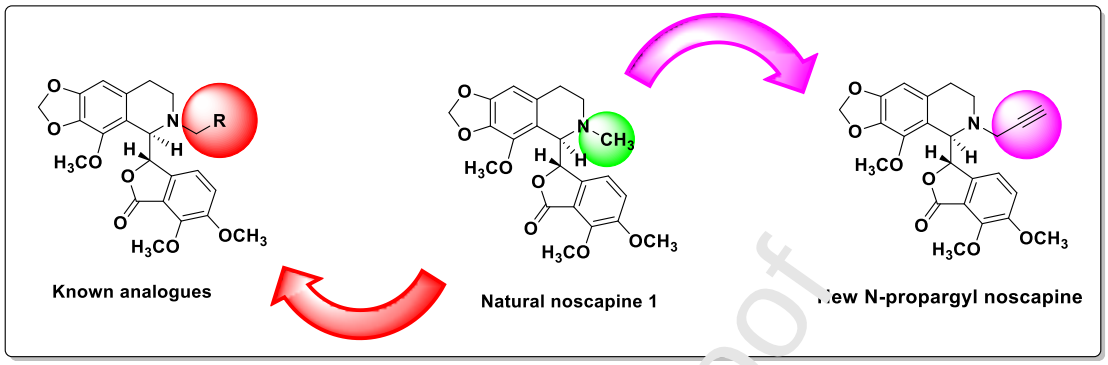

Figure 3B

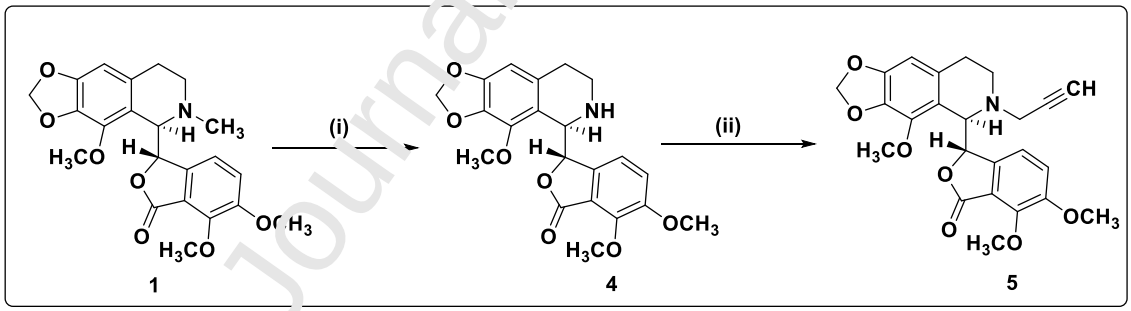

Figure 4

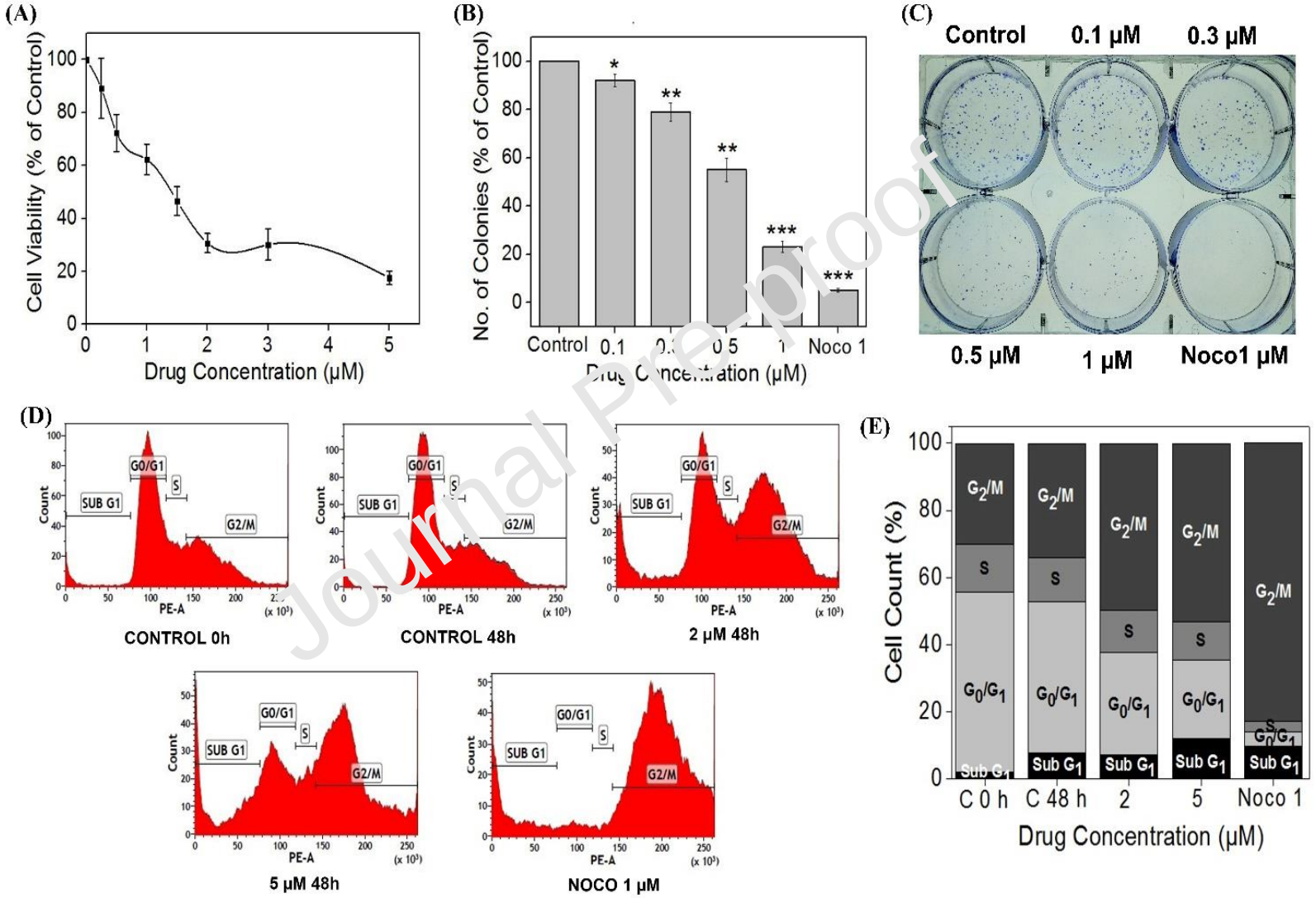

Figure 5

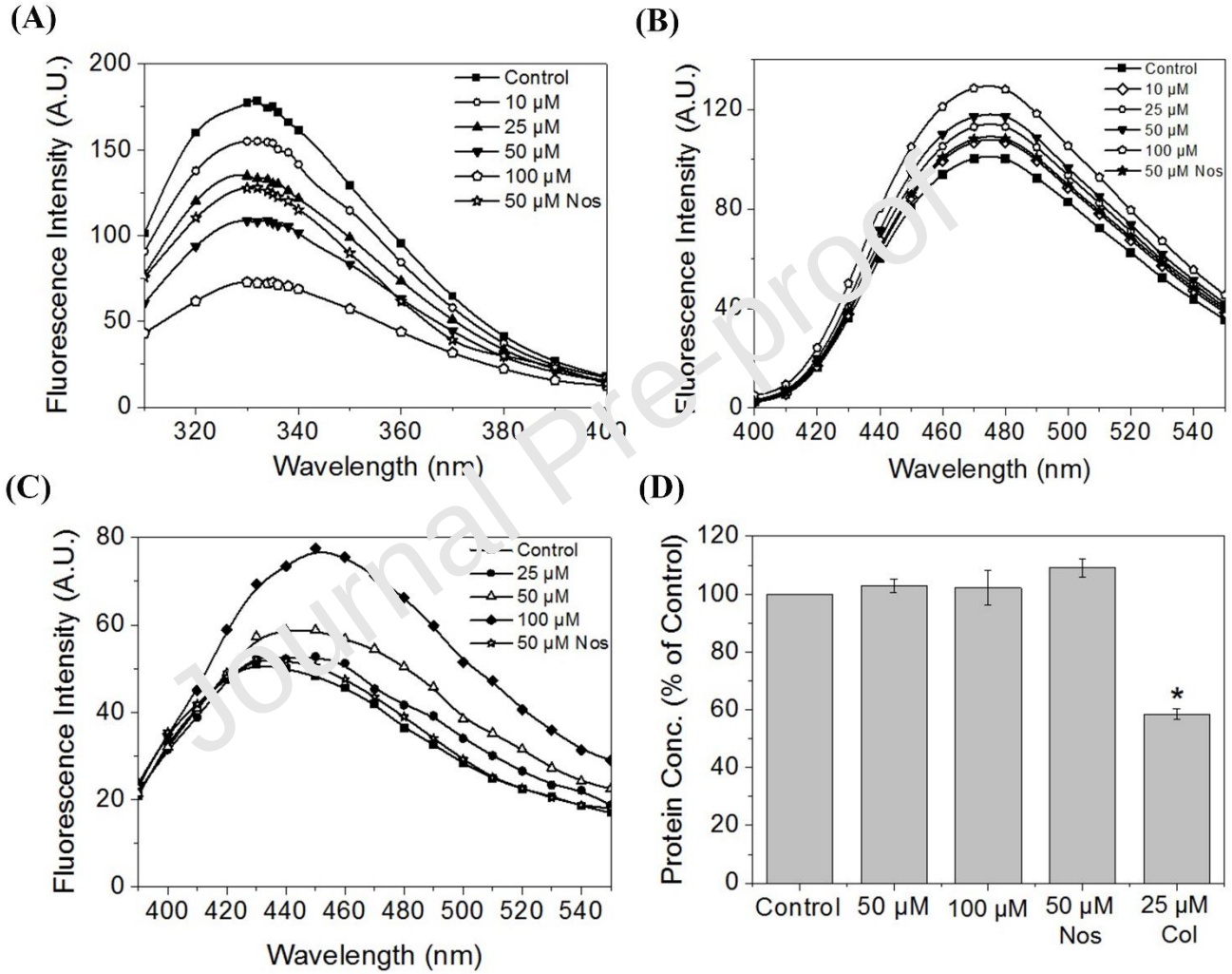

Figure 6

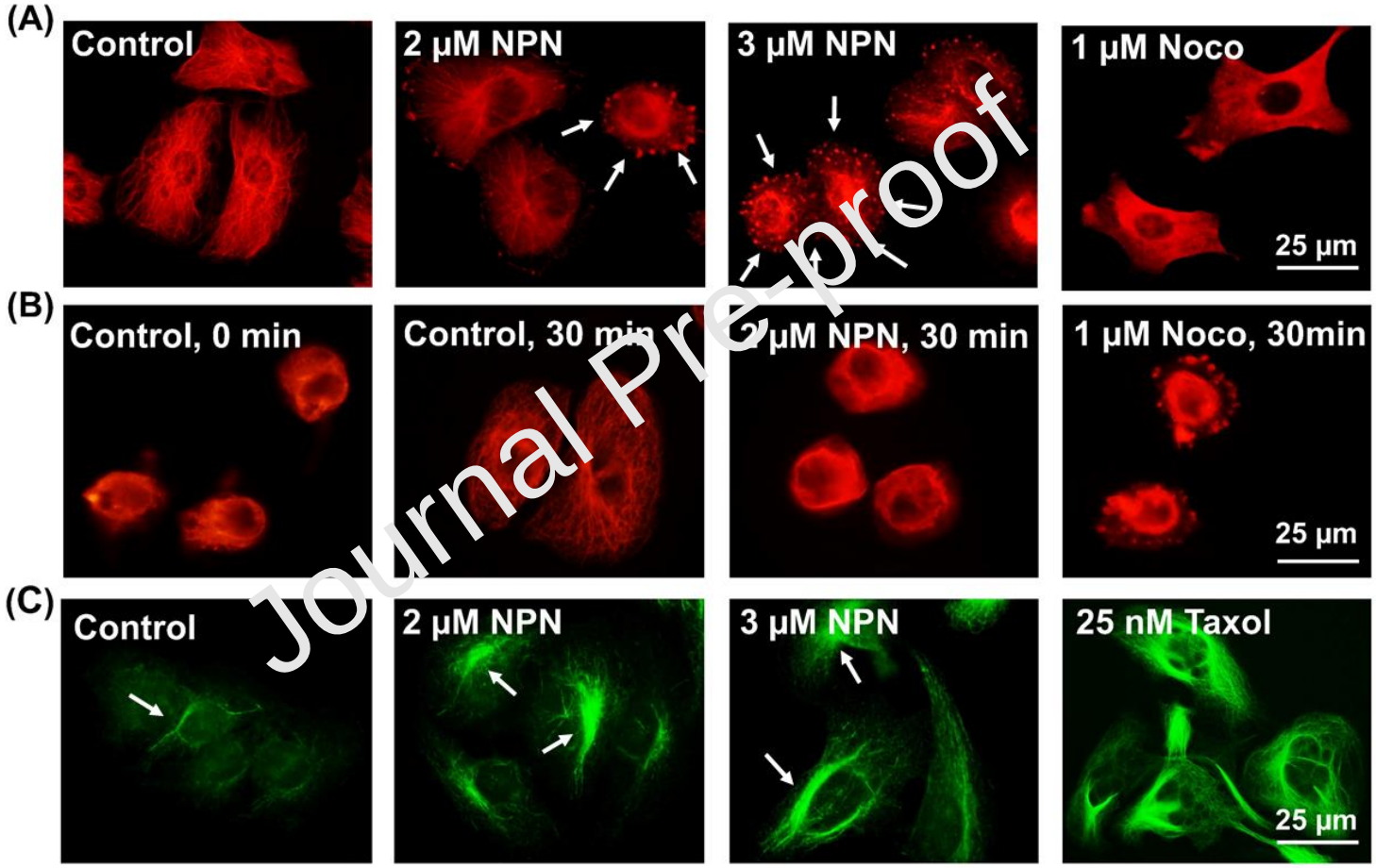

Figure 7

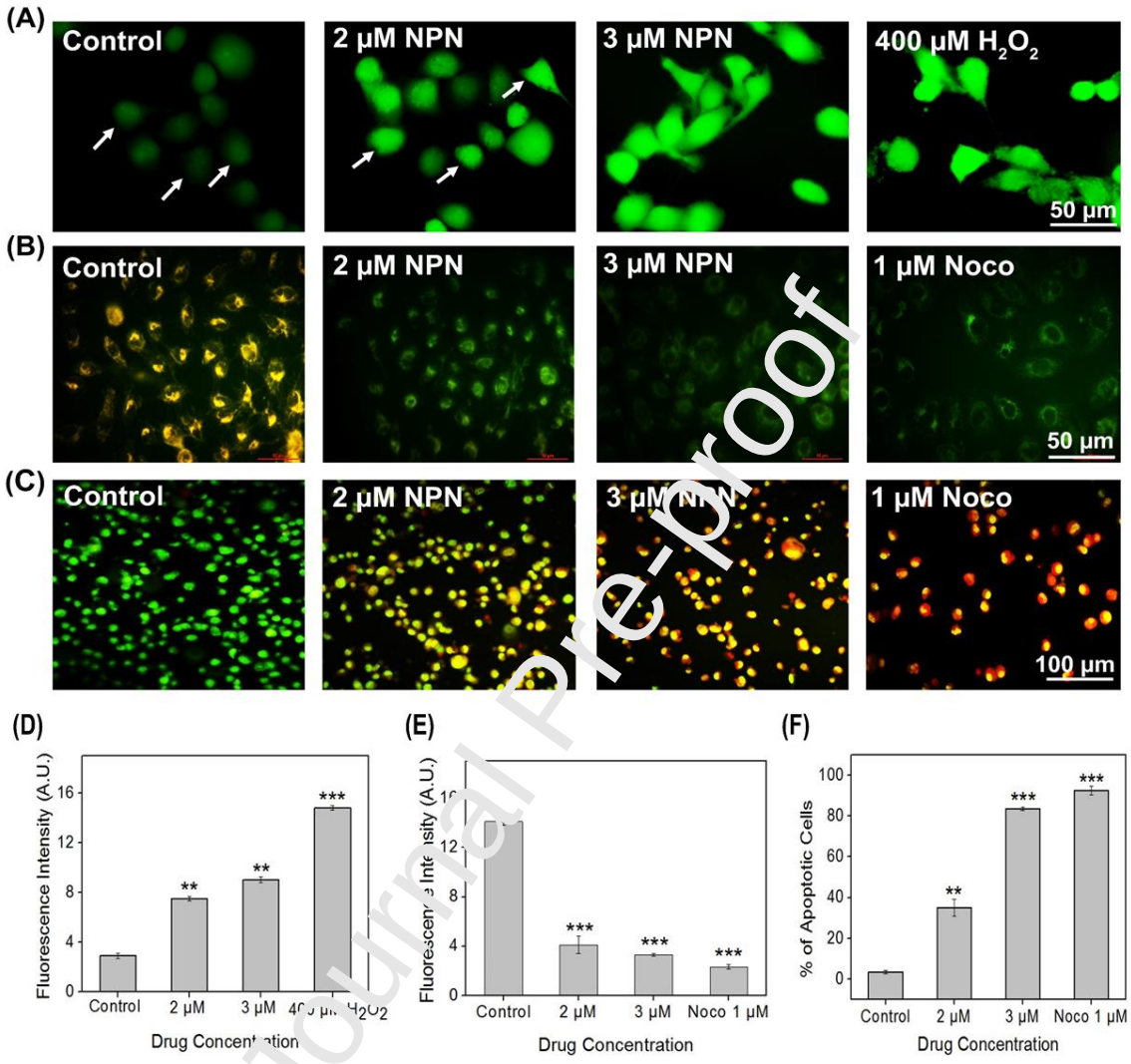

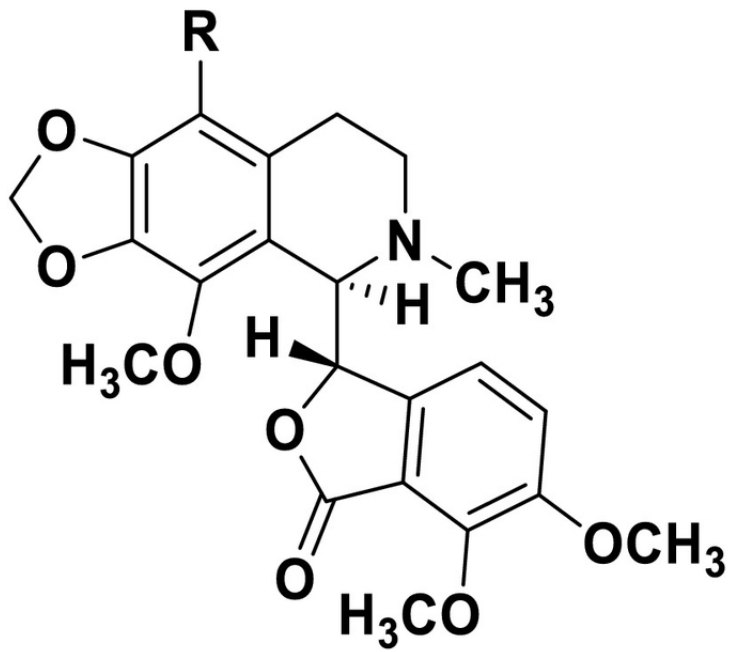

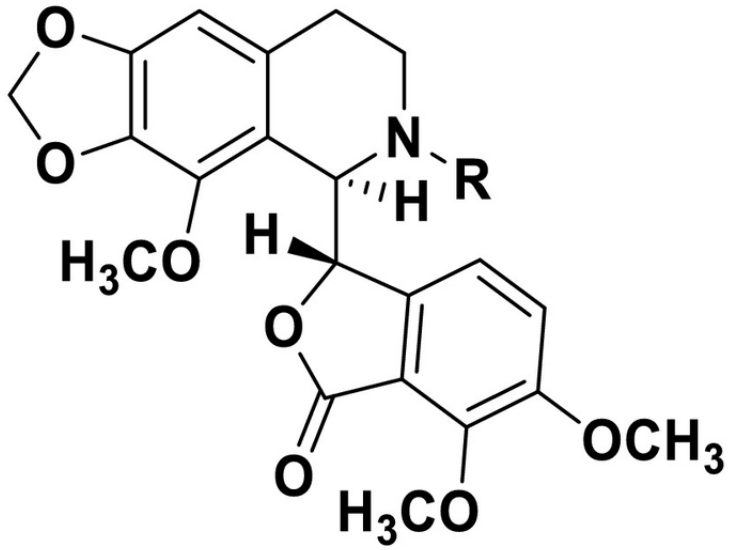

1: R =H; Natural Noscapine
2a: R =F; 2b: R =Cl; 2c: R =Br; 2d:R =I
2d: R =N_3;2e: R =NO_2; 2g: R=NH_2

3: R =Substituted benzyl groups; 3a: R=Substituted urea derivatives

Figure 1

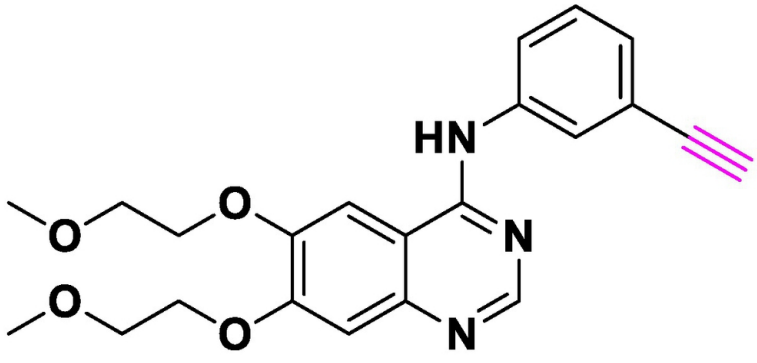

(I) Erlotinib

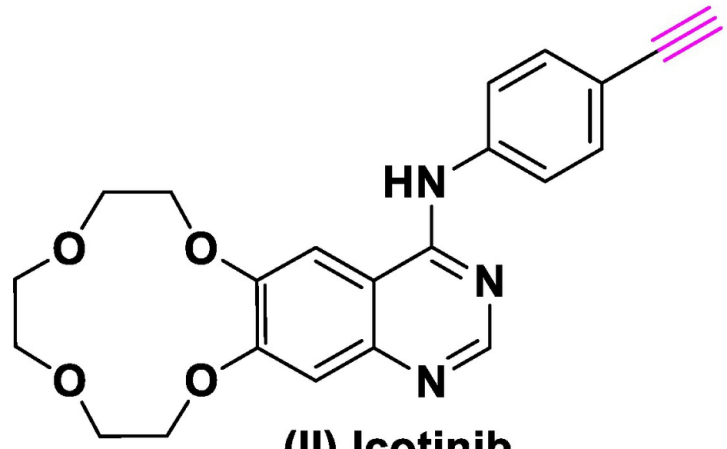

(II) Icotinib

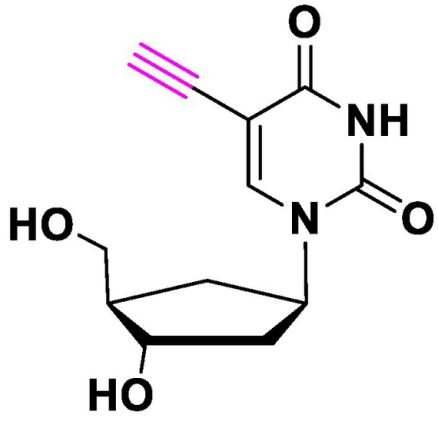

(III)

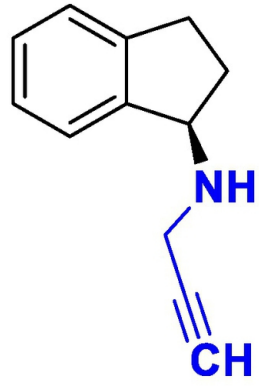

(IV) Rasagiline

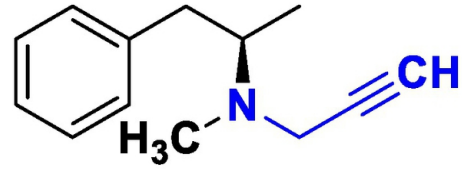

(V) Selegiline

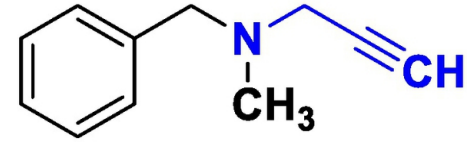

(VI) Pargyline

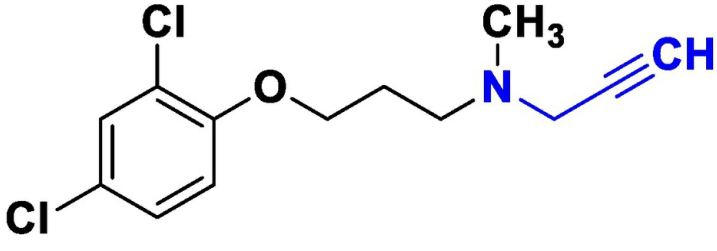

(VII) Clorgyline

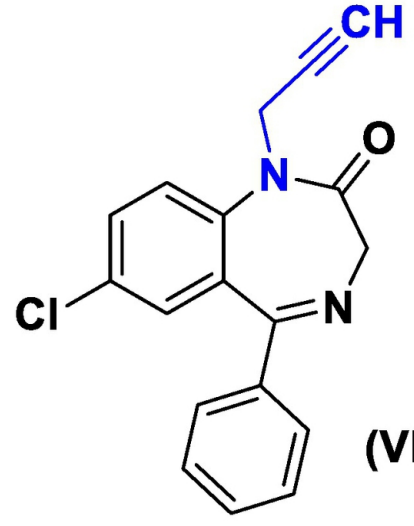

(VIII) Pinazepam

Figure 2

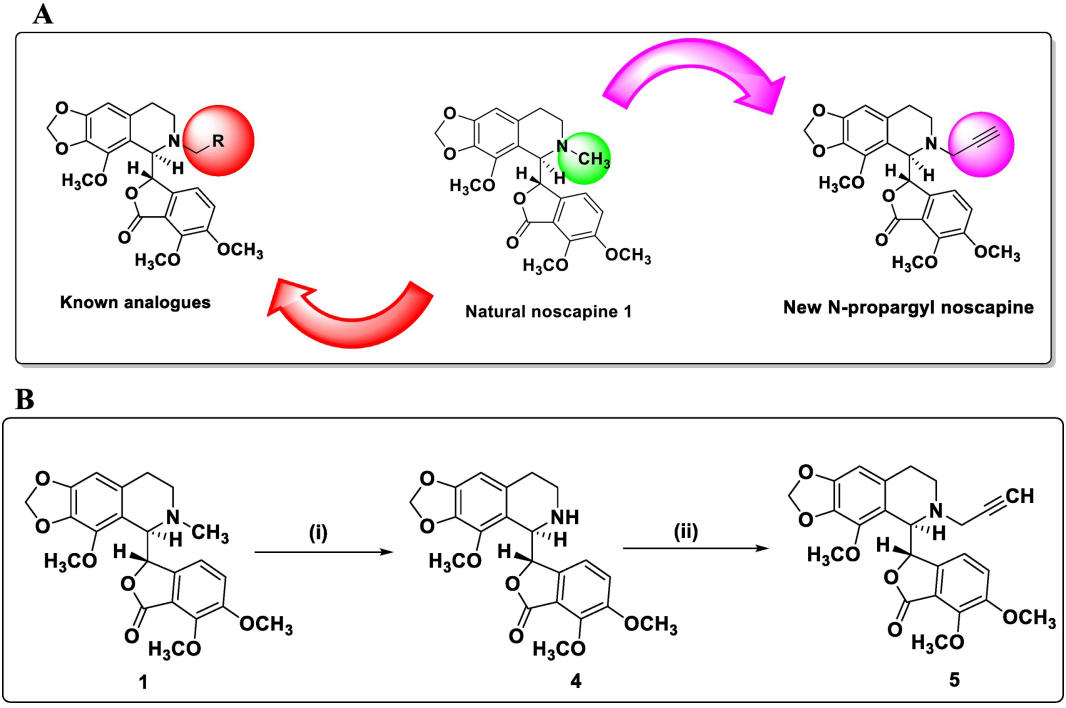
A
R
Known analogues
Natural noscapine 1
New N-propargyl noscapine
B
(i)
(ii)
1
4
5

Figure 3

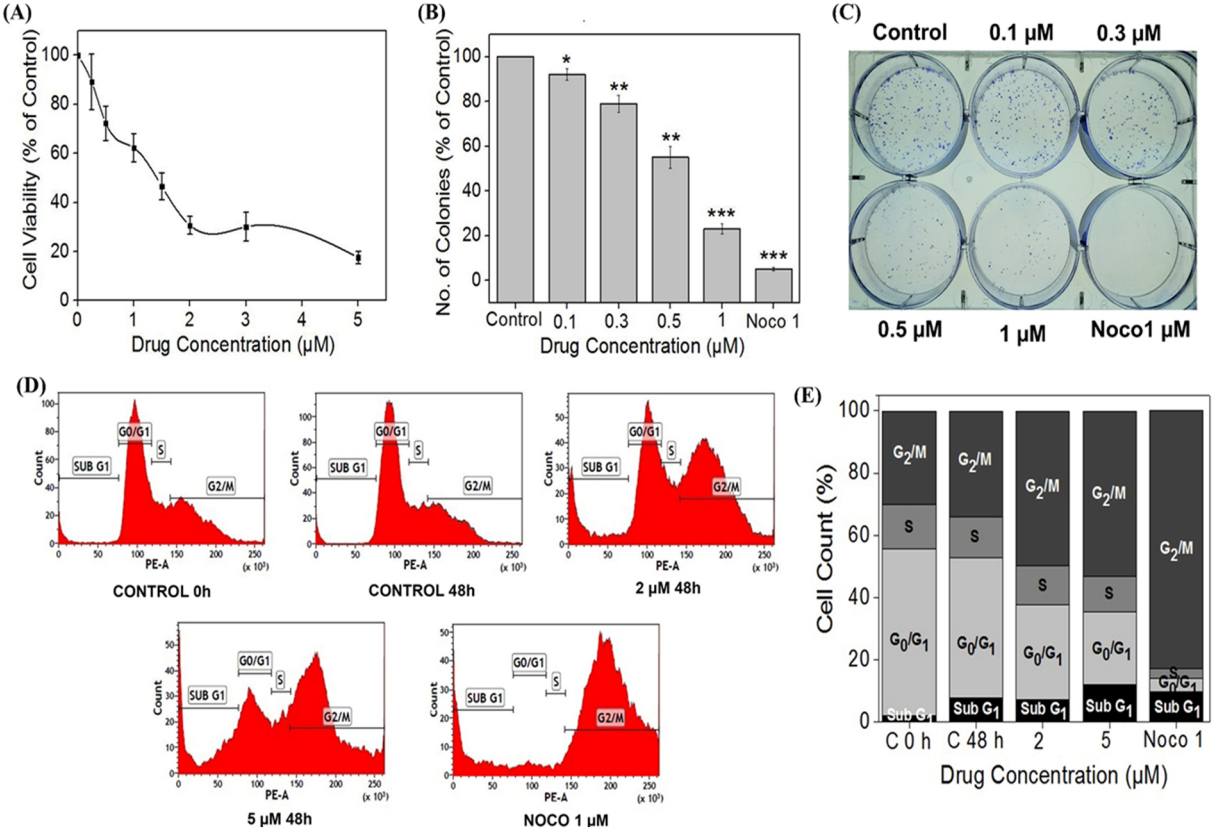
(A)
Cell Viability (% of Control)
Drug Concentration (μM)
(B)
No. of Colonies (% of Control)
Control
0.1
0.3
0.5
1
Noco 1
Drug Concentration (μM)
(C)
Control
0.1 μM
0.3 μM
0.5 μM
1 μM
Noco1 μM
(D)
SUB G1
G0/G1
S
G2/M
Count
PE-A
CONTROL 0h
CONTROL 48h
2 μM 48h
5 μM 48h
NOCO 1 μM
(E)
Cell Count (%)
G2/M
S
G0/G1
Sub G1
C 0 h
C 48 h
2
5
Noco 1
Drug Concentration (μM)

Figure 4

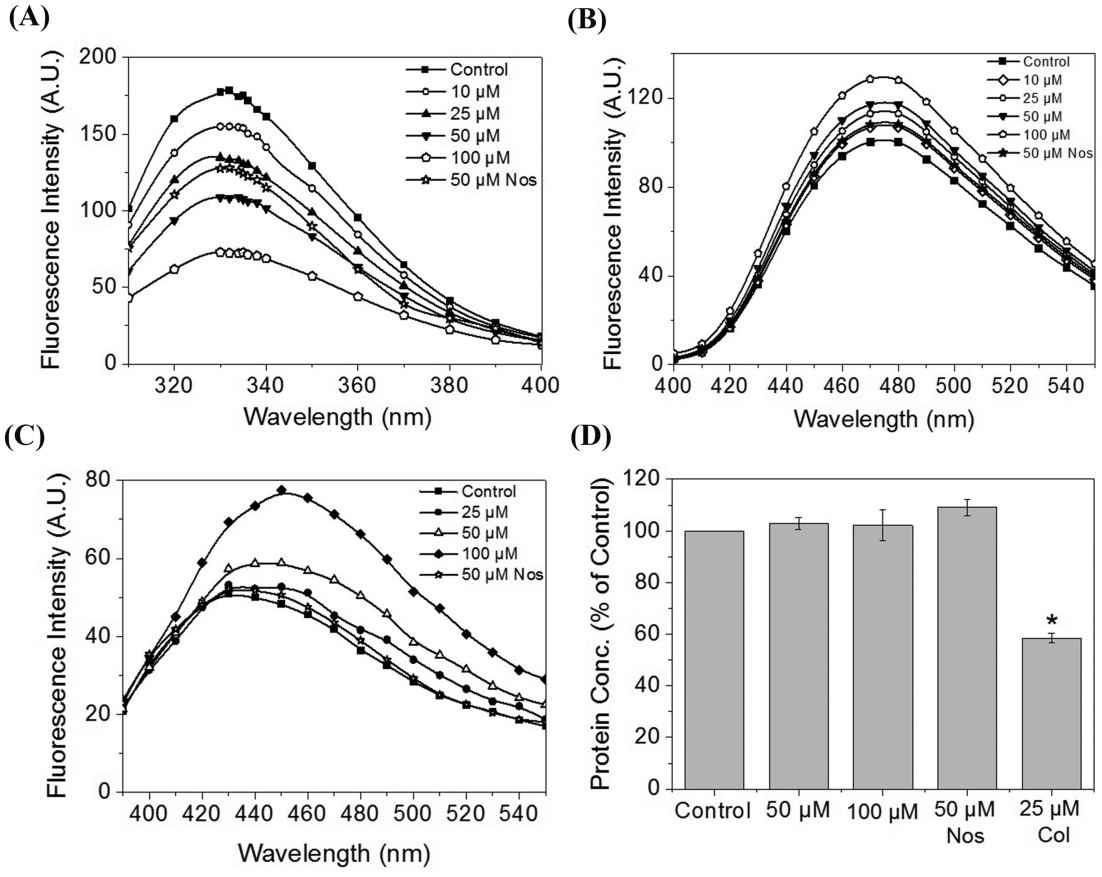
(A)
Fluorescence Intensity (A.U.)
Wavelength (nm)
Control
10 μM
25 μM
50 μM
100 μM
50 μM Nos
(B)
Fluorescence Intensity (A.U.)
Wavelength (nm)
Control
10 μM
25 μM
50 μM
100 μM
50 μM Nos
(C)
Fluorescence Intensity (A.U.)
Wavelength (nm)
Control
25 μM
50 μM
100 μM
50 μM Nos
(D)
Protein Conc. (% of Control)
Control
50 μM
100 μM
50 μM Nos
25 μM Col
*

Figure 5

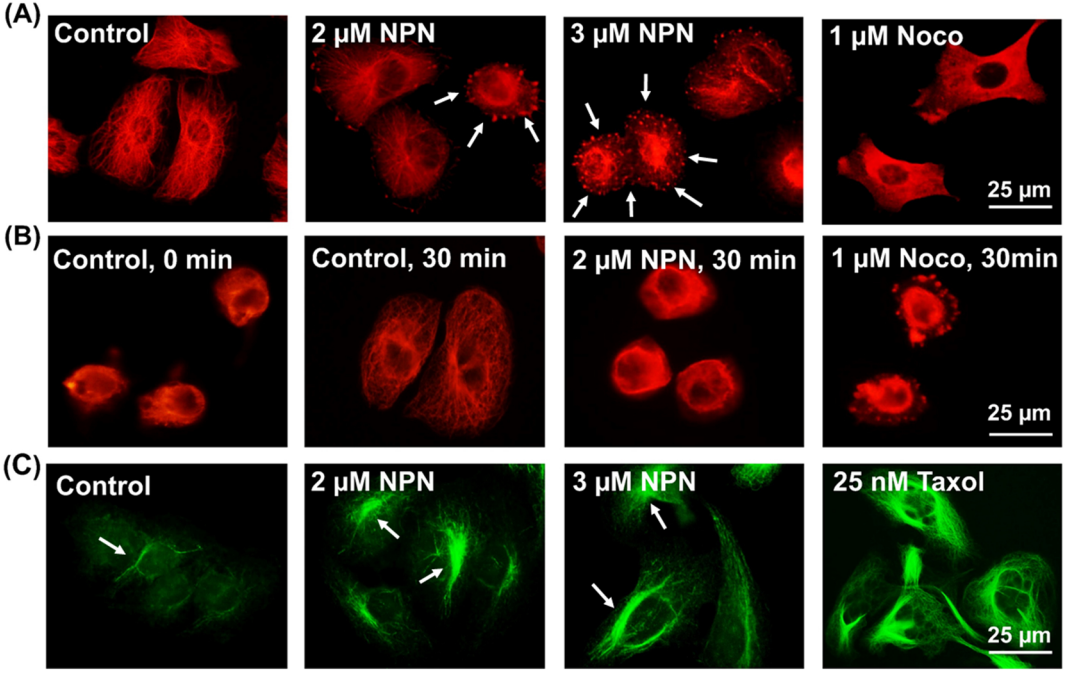
(A)
Control
2 μM NPN
3 μM NPN
1 μM Noco
25 μm
(B)
Control, 0 min
Control, 30 min
2 μM NPN, 30 min
1 μM Noco, 30min
25 μm
(C)
Control
2 μM NPN
3 μM NPN
25 nM Taxol
25 μm

Figure 6

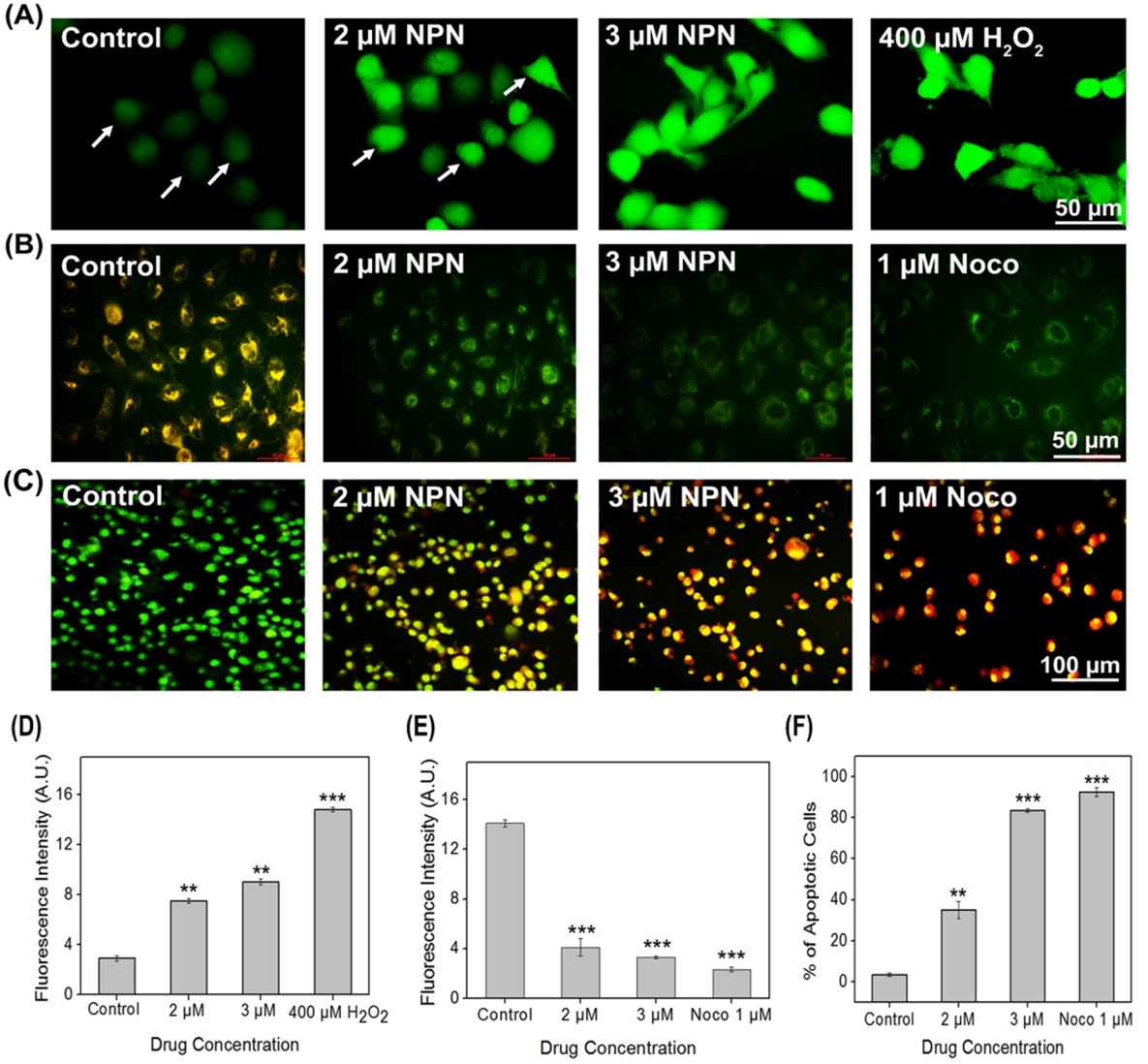
(A)
Control
2 μM NPN
3 μM NPN
400 μM H_2O_2
50 μm
(B)
Control
2 μM NPN
3 μM NPN
1 μM Noco
50 μm
(C)
Control
2 μM NPN
3 μM NPN
1 μM Noco
100 μm
(D)
Fluorescence Intensity (A.U.)
0
4
8
12
16
**
**
***
Control
2 μM
3 μM
400 μM H_2O_2
Drug Concentration
(E)
Fluorescence Intensity (A.U.)
0
4
8
12
16
***
***
***
Control
2 μM
3 μM
Noco 1 μM
Drug Concentration
(F)
% of Apoptotic Cells
0
20
40
60
80
100
**
***
***
Control
2 μM
3 μM
Noco 1 μM
Drug Concentration

Figure 7